Synergistic modulation of BiOI by atomic-level vacancies and dominant facets for efficient photocatalytic degradation of bisphenol A

Qicheng He, [a] Zhihao Zhang, [b] Quanxi Zhang, [b] * Zhifeng Zhang [a] *

[a] School of Life Science, Shanxi Normal University, Taiyuan 030031, China;

[b] Institute of Environmental Science, Shanxi University, Taiyuan 030006, China;

1. Experimental section

1.1 Characterizations

X-ray diffraction (XRD) patterns were recorded on an X-ray powder diffractometer (Ulitma IV, Japan) using Cu Kα radiation (40 kV, 40 mA, 10° min^{-1} from 5° to 90°). The morphological information of the samples was recorded on a field emission scanning electron microscope (JSM-7800F, Japan). The microstructure of the catalyst was characterized by field emission transmission electron microscopy (JEM-F200, Japan) (Acceleration voltage = 200 kV). X-ray photoelectron spectroscopy (XPS) was recorded on an x-ray photoelectron spectrometer (ESCALAB 250Xi) with Al Kα rays (hv = 1486.6 eV) as the excitation source (Working voltage = 14.6 kV). Charge correction was performed using C1s (284.8 eV) binding energy as the energy standard. All data were analyzed using Thermo Avantage v5.948 software. The reflectance spectra of the catalysts in the range of 200-800 nm were obtained by UV/Vis/NIR spectrophotometer (Hitachi U4150, Japan). Data related to photocurrent spectra and electrochemical impedance spectra (EIS) were recorded by testing with an electrochemical workstation (Zahner IM6, Germany). An electron paramagnetic

resonance (EPR) spectrometer (Bruke EMXPLUS, Germany) recorded electron paramagnetic resonance (EPR) spectra of spin-trapped paramagnetic substances. 5,5-dimethyl-1-pyrroline N-oxide (DMPO) was chosen as the probe for ·OH and $\cdot O_2^-$ and 4-Amino-2,2,6,6-tetramethylpiperidine (TEMP) as the probe for $^1O_2$ in the EPR test.

1.2 Positron annihilation spectra

TechnoAP positron lifetime measurement system was used for positron lifetime experiments with a time resolution of 200 ps. A ^{22}Na source of 20 μCi was sandwiched between two identical samples using a 70 μm thick Kapton package for a total count of over 3 million. The atomic superposition (ATSUP) method was used to construct the initial electron density, and the total positron electrostatic potential is constructed as the sum of the self-consistent nucleuses and electrons coulomb potential. Quantum Monte Carlo generalized gradient approximation (QMCGGA) method was used to calculate the positron-electron correlation potentials and the corresponding enhancement factor. And the positron wave functions are obtained with two-component of the density functional theory by the self-consistent finite difference method. A 3 ×1 ×3 supercells with 108 atoms was used to calculate the positron lifetime of vacancy-related vacancies structure in samples.

1.3 Theoretical calculation of different crystal planes

All the DFT results present in this work obtained using the Vienna ab initio simulation package (VASP) code. To solve the ion-electron interactions in the Kohn-Sham equations, we used the projector-augmented wave (PAW) method. The exchange correlation energy was calculated using the generalized gradient approximation with the Perdew-Burke-Ernzerhof functional (GGA-PBE). The Brillouin zone was sampled with a 1 × 1 × 1 k-point grid. BiOI (102) and BiOI (110) surface models all consist of periodic 2 × 2 four-layer slabs with a vacuum separation of 20 Å in the direction perpendicular to the surface (Figure 5b and 5f).

1.4 Theoretical calculation of different vacancy types

All the DFT calculations were conducted with a periodic slab model using the Vienna ab initio simulation program (VASP). The exchange and correlation energy were approximated by generalized gradient approximation (GGA) and the Perdew-Burke-Ernzerhof (PBE) functional. The projector augmented wave (PAW) method was used to describe the electrons-ion interaction. And the plane wave cutoff energy of 400 eV was utilized in the calculation of the compact convergence. A 20 Å vacuum region was used to ensure the intermolecular interaction between the slabs was negligible. The meshes of 1 × 1 × 1 k-points for the vacancies of $V_{BiOBiBi}$ and V_{BiIBi}. All the optimizations are converged with a force criterion of 0.035 eV/Å. The V_{BiIBi} was built by moving the two Bi atoms and one I atom of BiOI (102) surface, using a super-cell of size 2 x 2 and contains four layers (Figure 5j). The $V_{BiOBiBi}$ was built by moving the three Bi atoms and one O atom of BiOI (110) surface, using a super-cell of size 2 x 2 and contains four layers (Figure 5n). During all the calculations, the bottom two layers were fixed, while the other layers were allowed to relax.

2. Figure

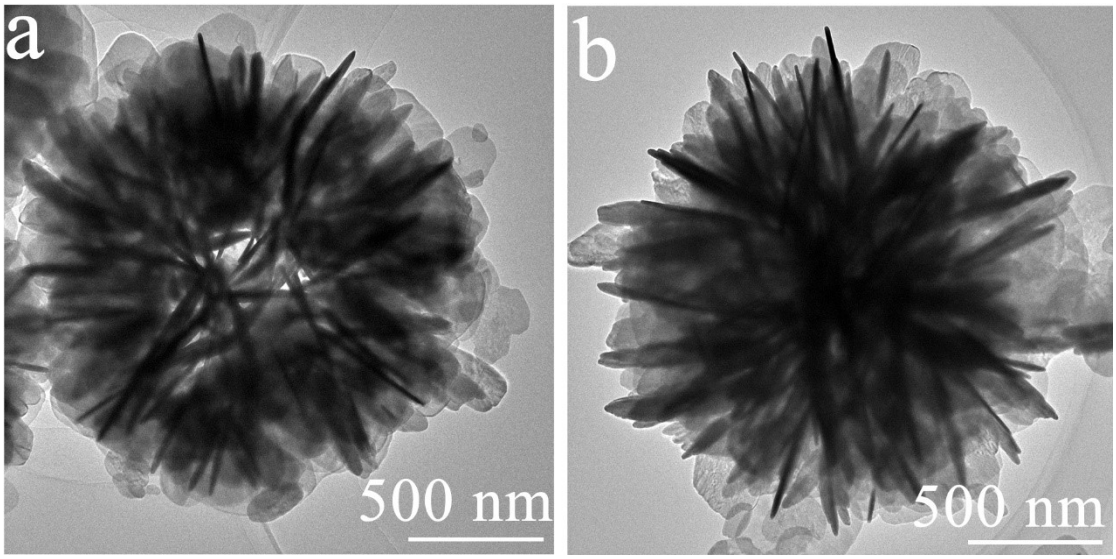

Figure S1. TEM images of (a) BiOI-1 and (b) BiOI-2.

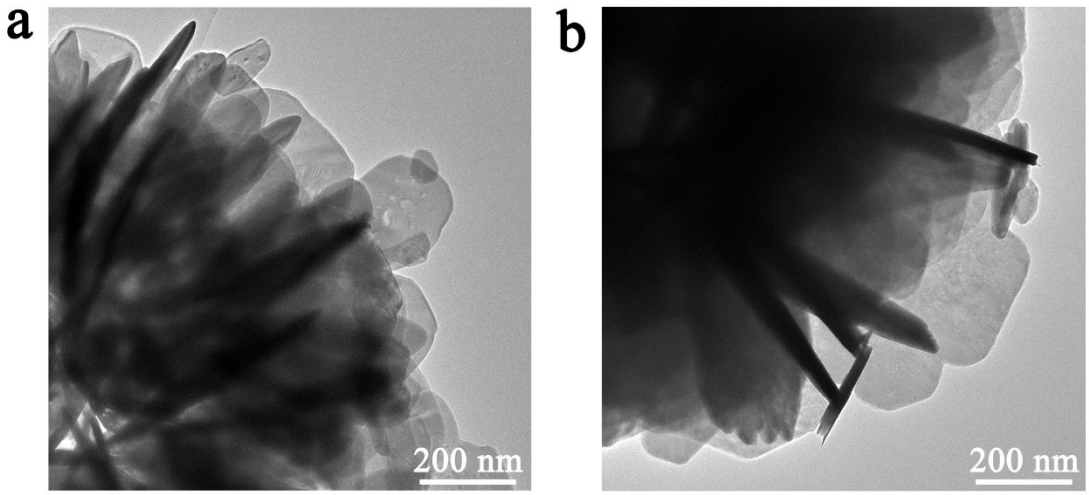

Figure S2. HRTEM images of BiOI-1 (a) low resolution; BiOI-2 (b) low resolution.

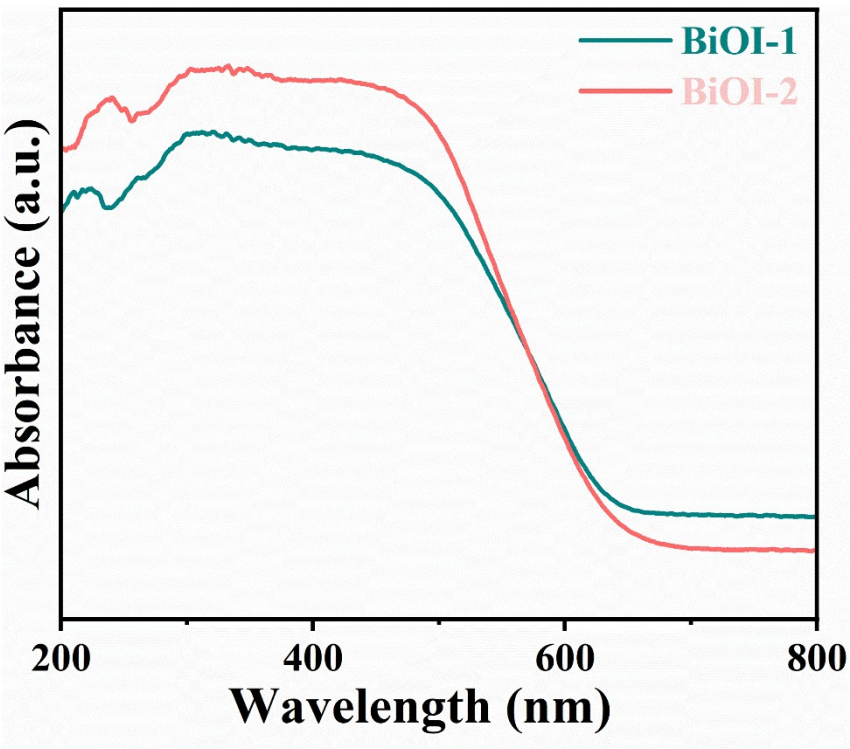

Figure S3. UV–vis absorption spectra of BiOI-1 and BiOI-2.

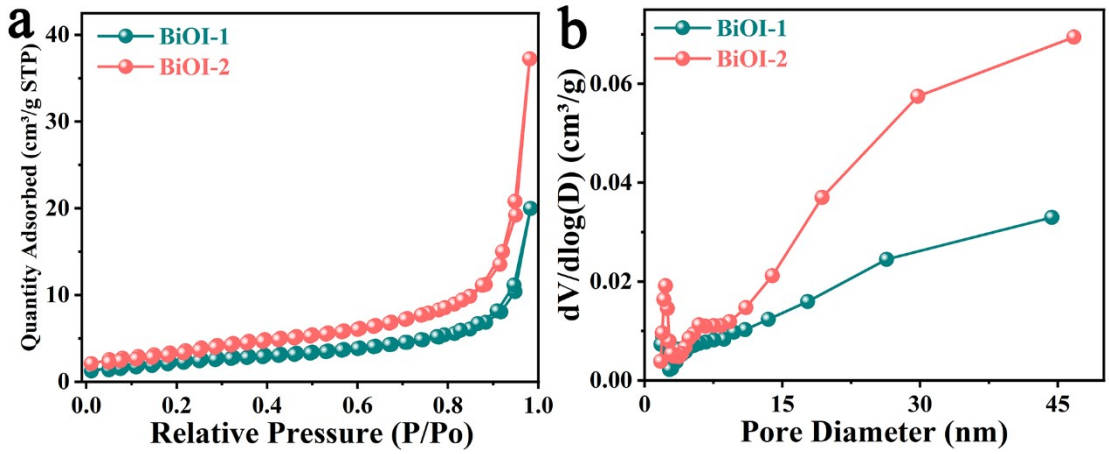

Figure S4. (a) Typical N_2 gas adsorption-desorption isotherms and (b) the corresponding pore size distribution of BiOI-1 and BiOI-2.

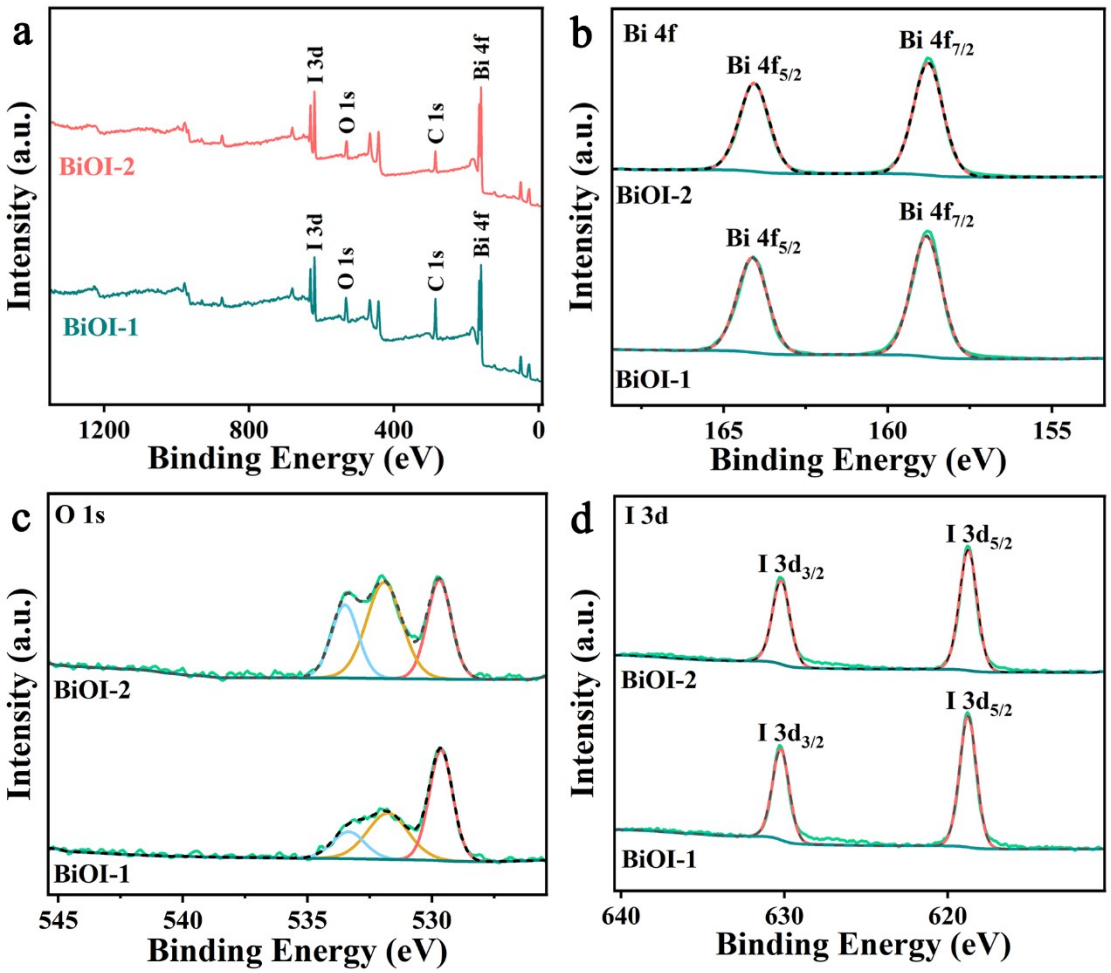

Figure S5. (a) XPS survey spectra; (b) Bi 4f spectra, (c) O 1s spectra, and (d) I 3d spectra of the as-synthesized catalysts.

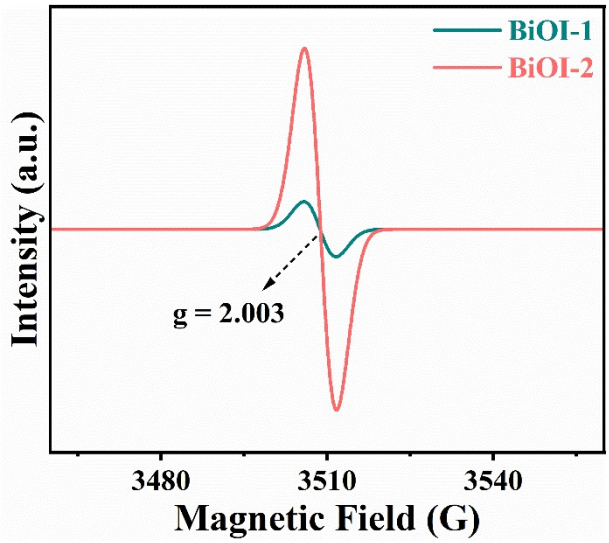

Figure S6. EPR spectra of BiOI-1 and BiOI-2.

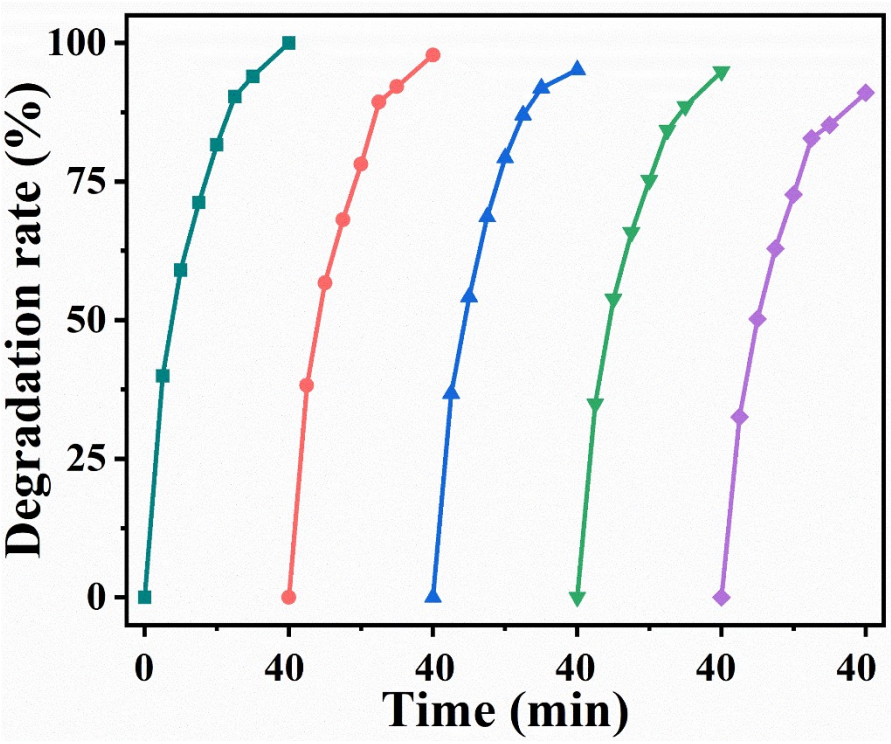

Figure S7. Cyclic degradation curve of BiOI catalyst. (BPA, 20 mg·L^{-1}; BiOI, 0.5 g·L^{-1})

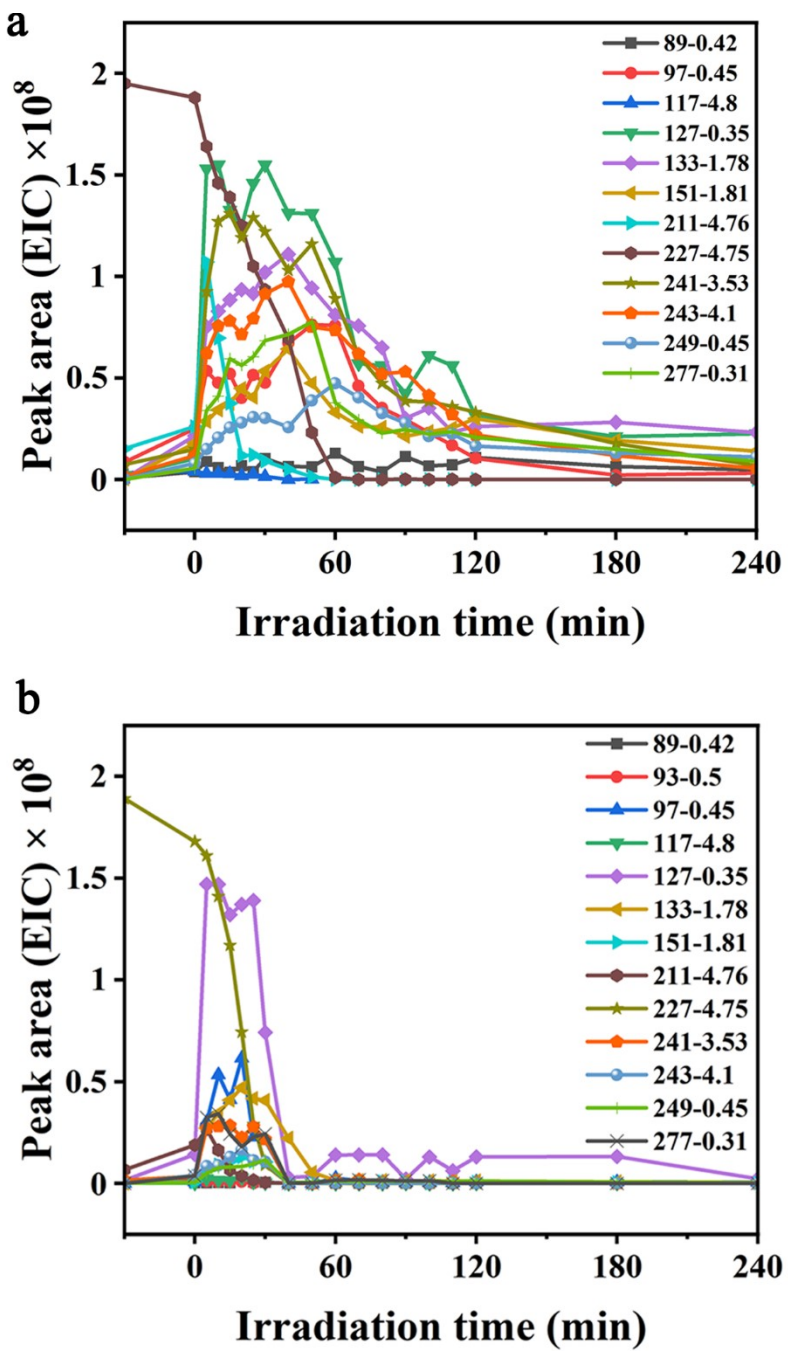

Figure S8. Evolution of product ions during photodegradation of BPA in presence of (a)BiOI-1and (b) BiOI-2.

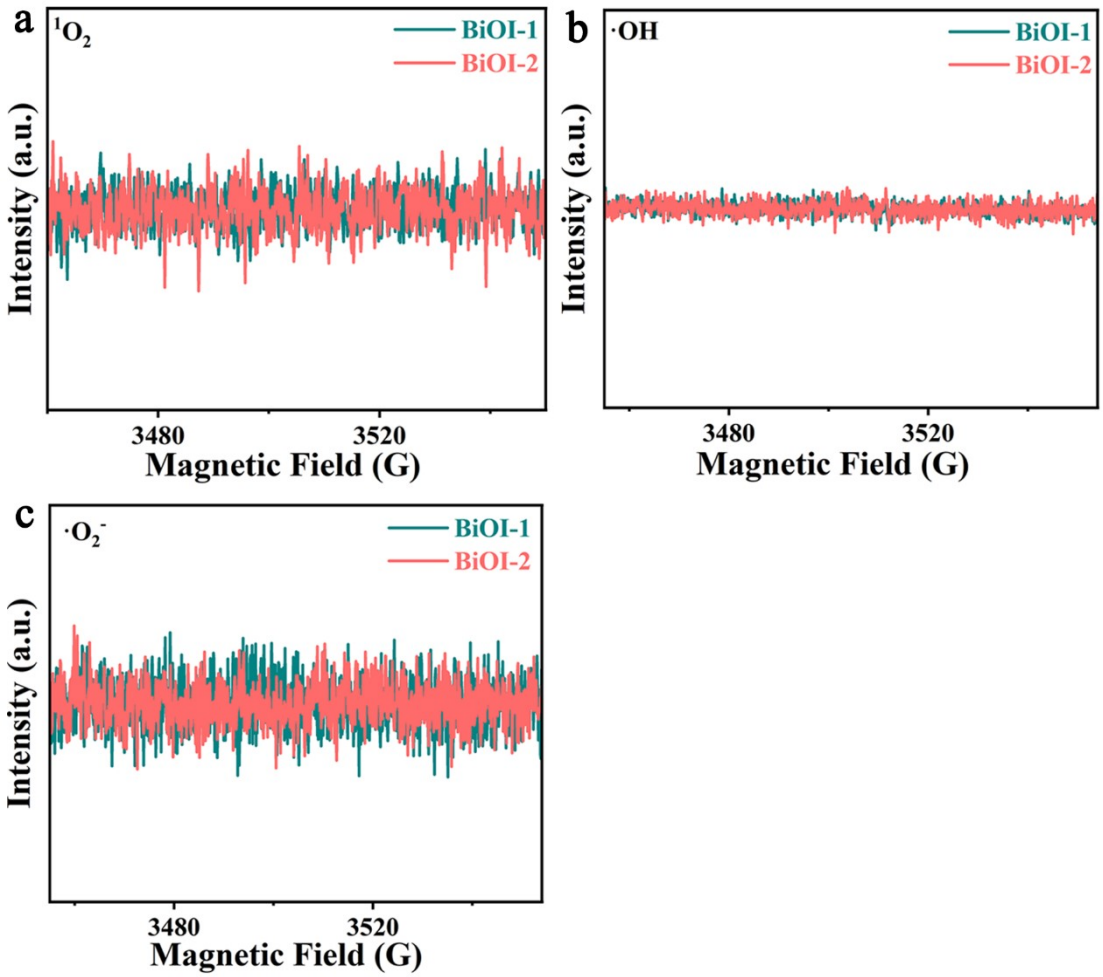

Figure S9. EPR spectra of (a) $^1O_2$, (b) ·OH, and (c) $\cdot O_2^-$ under dark condition

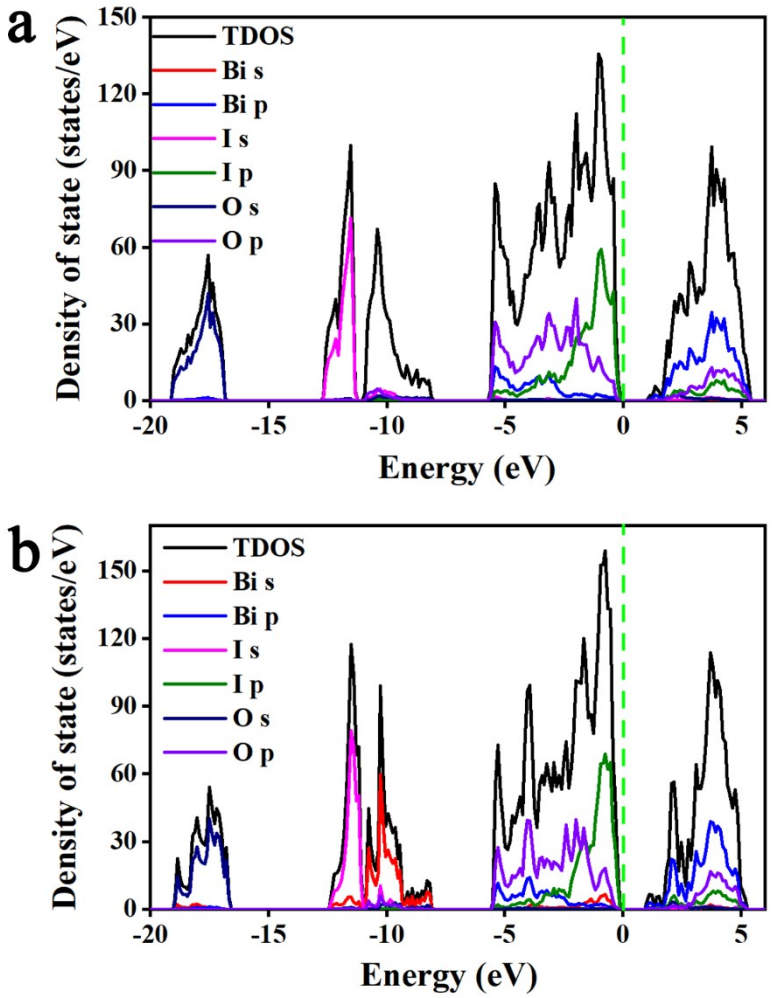

Figure S10. The density of states (DOS) of (a) BiOI (102) and (b) BiOI (110). (The green dash line represents the E_F.)

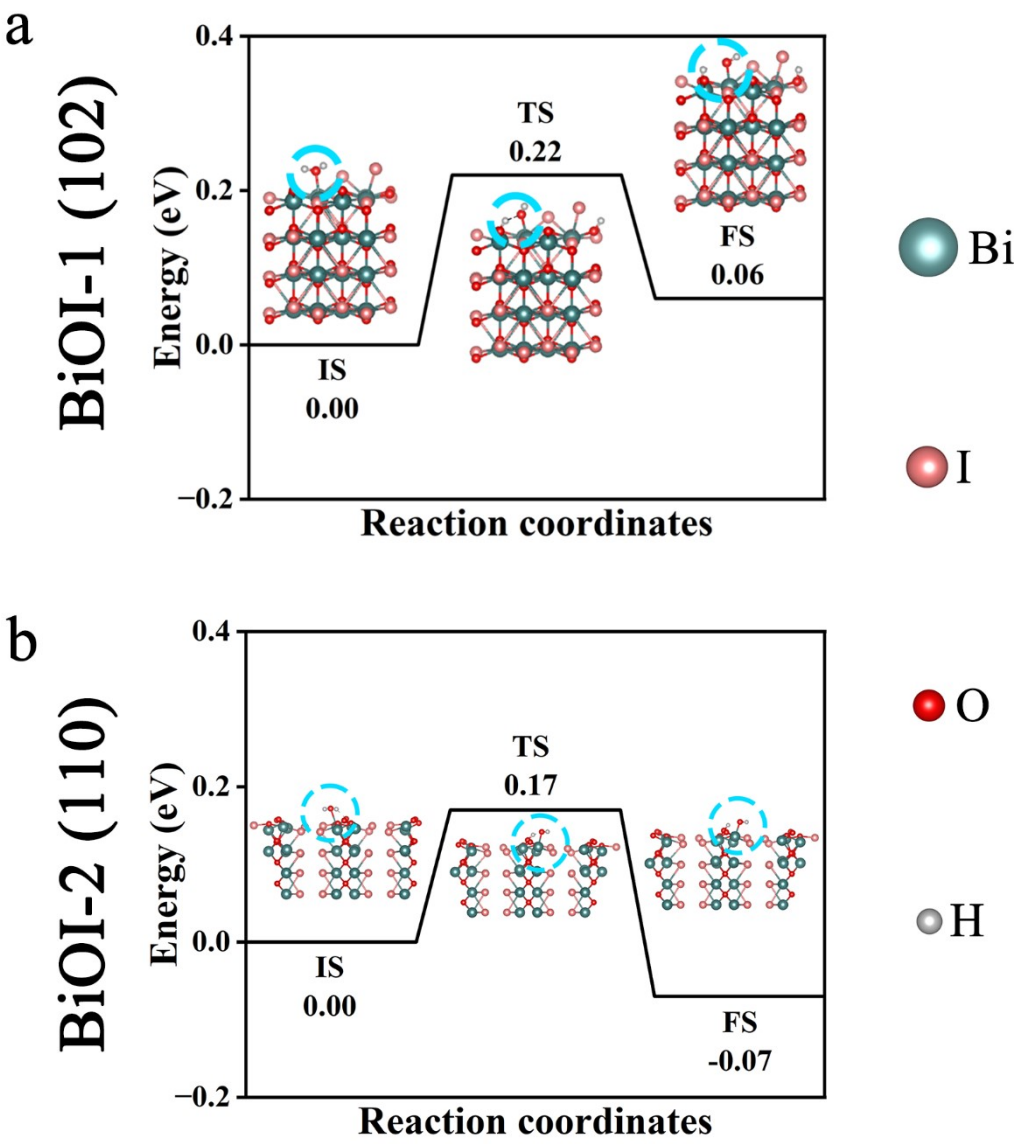

Figure S11. Optimized adsorption configuration of H_2O on (a) BiOI (102) and (b) BiOI (110).

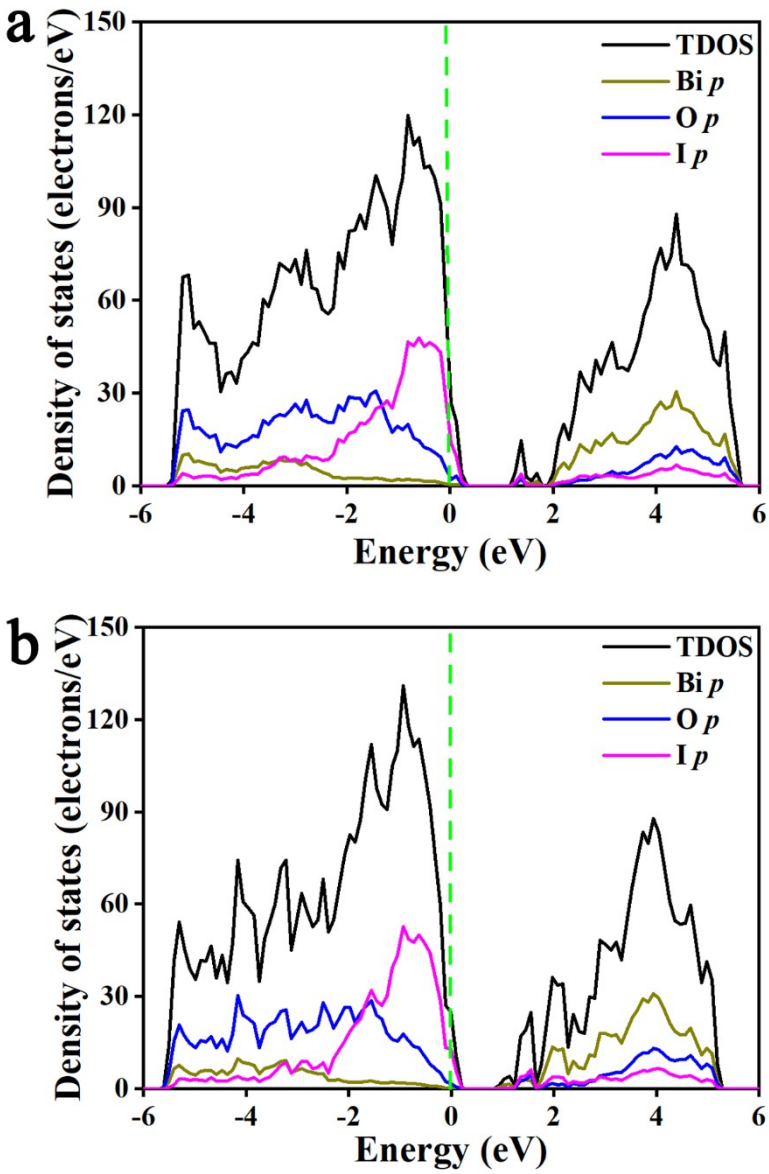

Figure S12. The density of states (DOS) of (a) BiOI (V_{BiIBi}) and (b) BiOI ($V_{BiOBiBi}$). (The green dash line represents the E_F.)

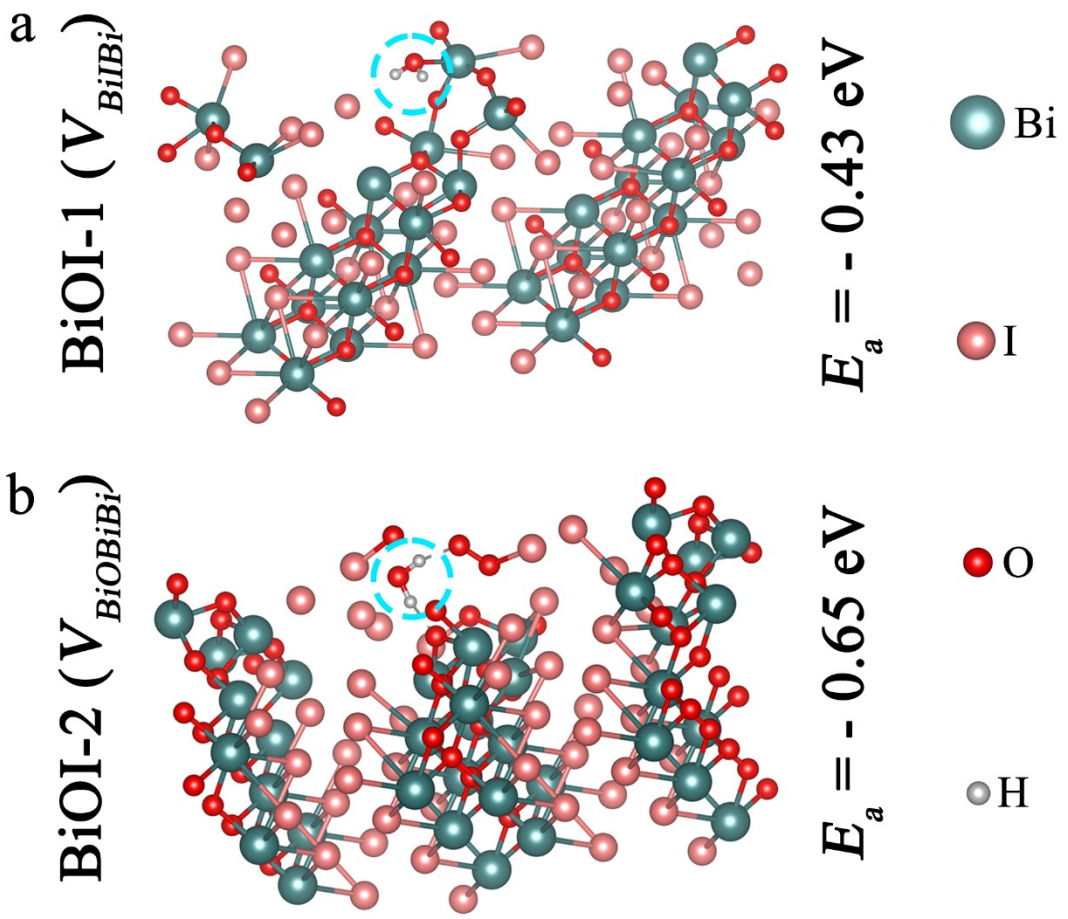

Figure S13. Optimized adsorption configuration of H_2O on (a) BiOI (V_{BiIBi}) and (b) BiOI ($V_{BiOBiBi}$).

3. Table

Table S1. The proportion of different exposed crystal planes.

Sample	$I_{(110)} / I_{(102)}$
BiOI-1	0.46
BiOI (PDF#10-0445)	0.63
BiOI-2	1.03

Table S2. N_2 adsorption-desorption data of as-synthesized catalysts.

Catalysts	BET Surface Area ($m^2 \cdot g^{-1}$)	Pore Size (nm)
BiOI-1	9.13	13.88
BiOI-2	14.45	15.63

Table S3. Positron Lifetime Parameters of Samples.

Samples	τ1 (ps)	τ2 (ps)	I1 (%)	I2 (%)
BiOI-1	325	765	94.5	5.5
BiOI-2	294	1591	95.2	4.8

Table S4. Calculated Positron Lifetime Values of Vacancies.

Structures	Perfect	V_{Bi}	V_I	V_{BiO}	V_{BiI}
Lifetime (ps)	273	275	299	276	311
Structures	V_{BiOBi}	V_{BiII}	V_{BiIBi}	$V_{BiOBiBi}$	$V_{BiIBiBi}$
Lifetime (ps)	281	349	326	290	340

Table S5. Identification of intermediates by LC-MS during BPA degradation.

	Compound name	Chemical structure	(m/z)	Retention time (min)
BPA	4,4'-(propane-2,2-diyl)diphenol	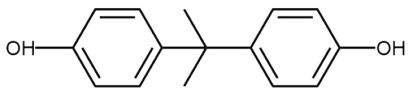	227	4.75

IP-1	4-(2-phenylpropan-2-yl)phenol		211	4.76
IP-2	4-(2-hydroxypropan-2-yl)phenol		151	1.81
IP-3	4-(prop-1-en-2-yl)phenol		133	1.78
IP-4	4-(2-(4-hydroxyphenyl)propan-2-yl)benzene-1,2-diol		243	4.1
IP-5	4-(2-(4-hydroxyphenyl)propan-2-yl)cyclohexa-3,5-diene-1,2-dione		241	3.53
IP-6	4-(3,4-dioxocyclohexa-1,5-dien-1-yl)-3-formyl-4-methylpentanoic acid		249	0.45
IP-7	(2E,4Z)-3-(2-(3,4-dihydroxyphenyl)propan-2-yl)hexa-2,4-dienedioic acid		277	0.31
IP-8	phenol		93	0.5
IP-9	oxalic acid		89	0.42
IP-10	hexa-1,5-dien-3-ol		97	0.45
IP-11	succinic acid		117	4.8
IP-12	heptanoic acid		127	0.35